Mathematical Biosciences 230 (2011) 12–22

Contents lists available at ScienceDirect

Mathematical Biosciences

journal homepage: www.elsevier.com/locate/mbs

Transport effects on surface reaction arrays: Biosensor applications

David A. Edwards

Department of Mathematical Sciences, University of Delaware, Newark, DE 19716-2553, USA

ARTICLE INFO

Article history:
Received 4 June 2010
Received in revised form 12 November 2010
Accepted 21 December 2010
Available online 1 January 2011

Keywords:
Surface-volume reactions
Rate constants
Asymptotics
Perturbation methods
Flexchip
dotLab

ABSTRACT

The ubiquity of surface-volume reactions in biological and industrial processes makes knowledge of their kinetics critical. This has spurred technological advances in several biosensors designed to measure rate constants, such as the Flexchip and the dotLab. These biosensors have multiple reacting zones in a single flow channel, and hence they also serve as good model systems for biochemical systems with multiple reacting zones, such as cell membranes. A correct mathematical model for such systems must incorporate the effects of transport and zone position. A basic unidirectional flow model is developed in general and solved for typical experimental parameters using perturbation methods. The effect of zone placement along the channel can be quantified in terms of an effective Damköhler number based upon position. Moreover, it is established that zone placement across the channel does not affect the measurements.

1. Introduction

In many important biological and industrial processes, chemical reactions occur where one of the reactants is attached to a solid surface. For instance, in the simplest bimolecular model, one reactant (the *ligand*) floats free in solution, while the other (the *receptor*) is affixed to the surface of a channel, cell membrane, etc. For example, immunoglobulins are transmitted to newborns from mother's milk through binding to receptors on intestinal epithelial cells [1]. Unfortunately, such reactions are not described by standard kinetics, as the components are not well-mixed.

Often these *surface-volume* reactions occur in the presence of an imposed flow, which can speed the reaction by continually replenishing the ligand supply. For example, flow reactors are more effective at synthesizing inorganic materials on templates [2]. In the food industry, alginate gel creation is enhanced by the addition of a convective flow of reactant [3]. A canonical biological example is clotting, where platelets adhere to foreign objects in the presence of blood flow [4]. In addition, many biological processes ensue when ligands floating in the bloodstream bind to receptors on the cell membrane [5].

In many industrial and biological contexts, the receptors are not confined to a single connected domain on the surface. Catalytic reactors may have multiple reacting zones on various catalytic wires [6]. Cell membranes may have multiple reacting zones in coated pits for the same ligand [7,8]. Lipid rafts are other structures on cell membranes that serve as localized reacting zones [9].

Creating a simple mathematical model of such complicated biological structures is daunting. Therefore, as a first attempt we model an experimental apparatus exhibiting the same geometry and dynamics: the Flexchip.

1.1. The Flexchip

Scientists have long known the importance of understanding the kinetics for such surface-volume reactions. To that end, several competing optical biosensors have appeared on the market to measure rate constants for a given reaction in real time without disturbing the underlying system. These biosensors have quickly grown in popularity, as indicated by the fact that over 1000 papers each year feature their use [10,11]. The configuration of such devices is described in great detail elsewhere [12–14]. For our purposes, it will be convenient to think of such a biosensor as a device where ligand in solution is convected over a reacting zone, and the process of the reaction is measured optically so as not to disturb it.

Over time, the technology has improved so that multiple reacting zones can be measured at once, enabling enhanced data collection of the same or different reactions without resetting the equipment. As a canonical example of such technology, we will study the Flexchip made by BIAcore [15,16], though we shall show in Section 5 that the same mathematical model also applies to the dotLab, made by Axela [13].

The Flexchip is shown in Figs. 1 and 2. An array of circular zones of diameter L_r is fabricated on the floor of a channel, which has length L_f, width W, and height H. For the purposes of this paper,

E-mail address: edwards@math.udel.edu

0025-5564/$ - see front matter © 2011 Elsevier Inc. All rights reserved.
doi:10.1016/j.mbs.2010.12.006

Nomenclature

Variables and parameters

Units are listed in terms of length (L), mass (M), moles (N), or time (T). If the same letter appears both with and without tildes, the letter with a tilde has dimensions, while the letter without a tilde is dimensionless. The equation where a quantity first appears is listed, if appropriate.

$\widetilde{B}(\tilde{x},\tilde{z},\tilde{t})$	bound ligand concentration in reacting zone on surface $\tilde{y}=0$, units N/L^2 (2.11)
$\widetilde{C}(\tilde{x},\tilde{y},\tilde{z},\tilde{t})$	unbound ligand concentration, units N/L^3 (2.5)
D	molecular diffusion coefficient, units L^2/T (2.5)
Da	Damköhler number, which measures the ratio of reaction and diffusion effects (2.7)
H	height of the channel, units L
$h(\cdot)$	function characterizing the effect of geometry and flow (3.9)
$I(x,z_{\mathrm{f}})$	indicator function for reacting zone (2.15a)
i	indexing variable for the $\tilde{x}$-position of a reacting zone
j	indexing variable for the $\tilde{z}$-position of a reacting zone
K	normalized affinity constant for system, defined as $k_{\mathrm{off}}/k_{\mathrm{on}}C_{\mathrm{u}}$ (2.13b)
k_{off}	dissociation rate, units T^{-1} (2.11)
k_{on}	binding rate, units L^3/NT (2.7)
L	dimensional length, variously defined, units L
n	indexing variable
$\widetilde{P}(\tilde{x})$	pressure in channel, units M/LT^2 (2.1)
Pe	Péclet number for the system, defined as VH^2/DL_{r} (2.6b)
Q	flow rate through channel, units L^3/T
R	total number of receptor sites, units N/L^2 (2.11)
Re	Reynolds number for system (A.1)
$\mathcal{S}_{ij}[B]$	sensogram signal from the ijth reacting zone (2.16)
$\tilde{t}$	dimensional time, units T (2.5)
V	four times the (maximal) velocity of flow at center of channel, units L/T (2.3)
$\tilde{v}(\tilde{y},\tilde{z})$	flow velocity, units L/T (2.1)
W	width of the channel, units L
$\tilde{x}$	dimensional measure of length along the channel, units L
$\tilde{y}$	dimensional measure of height above the binding surface, units L (2.1)
$\mathcal{Z}$	the integers
$\tilde{z}$	dimensional measure of length transverse to channel flow, units L
α	dimensionless constant, defined as $1+K$ (2.18a)
β	function characterizing z-dependence of signal (4.15)
ϵ	aspect ratio of the channel, defined as H/W (2.4)
κ	ratio of convective time scale to reaction time scale (2.8b)
μ	bulk viscosity, units M/LT (2.1)
ν	kinematic viscosity, units L^2/T (A.1)
ξ	dummy variable (3.6)

Other notation

f	as a subscript, used to indicate the flow channel
n	as a subscript, used to indicate a nonreacting zone
$n\in\mathcal{Z}$	as a subscript on B, used to indicate an expansion in Da (3.7)
r	as a subscript, used to indicate the reacting zone (2.11)
s	as a subscript, used to indicate a steady state (2.18a)
u	as a subscript on C, used to indicate its upstream value (2.7)
Δ	used to indicate a displacement (2.2)
∞	as a subscript on h, used to indicate the outer solution (3.9)
$-$	as a superscript, used to indicate the lower endpoint of a range
$+$	as a superscript, used to indicate the upper endpoint of a range

we will consider a rectangular array, as in [15]. However, hexagonal arrays are also used [17].

The flow in the Flexchip is laminar (see the Appendix for an estimate of the Reynolds number), and due to its small height, the flow is parabolic in the cross-section shown in Fig. 2 (see the next section for a formal justification). Receptors are attached to the channel floor in distinct zones, shown in Fig. 2 as $\tilde{x}\in[\tilde{x}_i^-,\tilde{x}_i^+]$. An evanescent wave is bounced off the channel floor and read by a detector. As the experiment progresses, binding causes refractive changes to the polarized light beam. These changes, when compared to a control state, can be translated into a *sensogram* of the binding [12].

This experimental setup can be viewed as a natural generalization of earlier-generation BIAcore SPR devices, which had only one reacting zone. These devices, which we shall refer to as "1-zone BIAcore", have been widely studied (cf. [18–21]). However, with the addition of multiple reacting zones, the effects of ligand depletion from upstream zones becomes more subtle.

In the next section we present the general governing equations that hold in systems of this type. We then specialize to the common experimental case where the Damköhler number Da is small. Using a perturbation analysis, we demonstrate that the effects of zone position in the $\tilde{x}$- and $\tilde{z}$-directions decouple. The *floor layer* solution characterizes the effect of the zone's position *along* the channel in the $\tilde{x}$-direction. The effect is related to depletion, and hence the results are similar to those obtained for the 1-zone BIAcore. In particular, the effect of position along the channel can be characterized by a single parameter, the effective Damköhler number. The *wall layer* solution characterizes the effect of the zone's position *across* the channel in the $\tilde{z}$-direction, and we establish that such effects are negligble.

2. Governing equations

2.1. The flow field

Due to the placement of the channel with respect to the inlet and outlet, in general the flow field in the Flexchip can be quite complicated [15]. However, as a first approximation we neglect these effects by treating the channel length L_{f} as much longer than the distance from the ends to the inlet and outlet. This leads to a unidirectional steady velocity field $\tilde{v}$ in the $\tilde{x}$-direction. We summarize the evolution equations for such a field; interested readers may find the details in [22], p. 72, for example.

By conservation of mass, a flow only in the $\tilde{x}$-direction will not depend on $\tilde{x}$. Also, with no velocity components in the other directions, the pressure $\widetilde{P}$ will depend *only* on $\tilde{x}$. Hence only the conservation of $\tilde{x}$-momentum equation contributes to the system:

$$\mu\left(\frac{\partial^2\tilde{v}}{\partial\tilde{y}^2}+\frac{\partial^2\tilde{v}}{\partial\tilde{z}^2}\right)=\frac{d\widetilde{P}}{d\tilde{x}}, \tag{2.1}$$

where μ is the viscosity of the fluid. But the left-hand side of (2.1) is a function of $\tilde{y}$ and $\tilde{z}$, and the right-hand side is a function of $\tilde{x}$. Hence both sides must be constant and we have

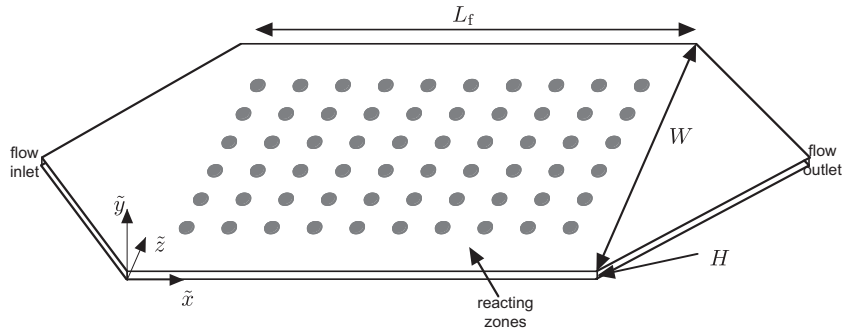

Fig. 1. Schematic of Flexchip. Though the reacting zones in the device are circles, we shall model them as rectangles for simplicity.

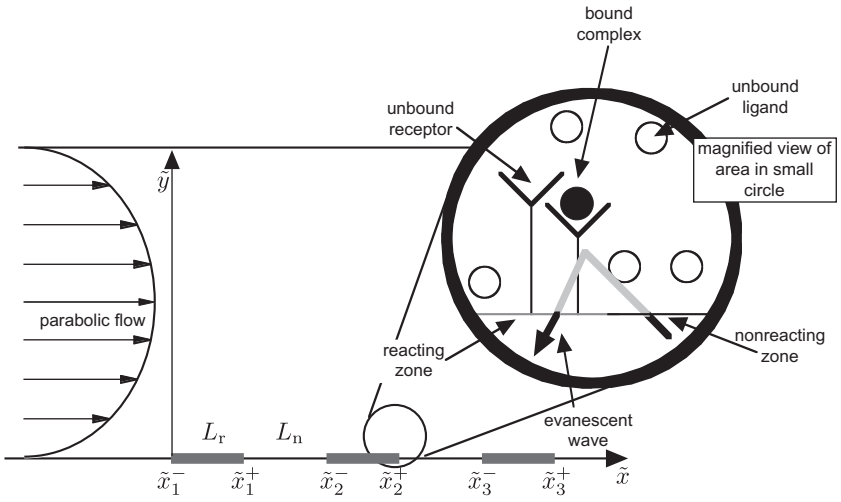

Fig. 2. Model of Flexchip, side view.

$$\mu\left(\frac{\partial^2\tilde{v}}{\partial\tilde{y}^2}+\frac{\partial^2\tilde{v}}{\partial\tilde{z}^2}\right)=-\frac{\Delta P}{L_f}, \tag{2.2}$$

where ΔP is the constant pressure differential that describes the effect of the pressure on the velocity field; the actual pressure $\tilde{P}$ is not needed in the analysis.

In order to simplify the problem, we use dimensionless variables. Hence we introduce the following scalings:

$$v_f(y_f,z_f)=\frac{\tilde{v}(\tilde{y},\tilde{z})}{V},\quad V=\frac{H^2\Delta P}{2\mu L_f},\quad y_f=\frac{\tilde{y}}{H},\quad z_f=\frac{\tilde{z}}{W}. \tag{2.3}$$

Substituting (2.3) into (2.2), we obtain

$$\left(\frac{\partial^2 v_f}{\partial y_f^2}+\epsilon^2\frac{\partial^2 v_f}{\partial z_f^2}\right)=-2,\quad 0\leqslant y_f\leqslant 1,\quad 0\leqslant z_f\leqslant 1;\quad \epsilon=\frac{H}{W}. \tag{2.4}$$

The mathematical discussion above may lead one to believe that once given ΔP, we would then calculate the appropriate V for scaling purposes. However, in a typical experimental setup we know neither ΔP nor V, but rather the flow rate Q. In the next section we will derive a simple relationship between Q and V; also ΔP drops out of our analysis completely once V is known.

2.2. Ligand transport and the floor layer

With our unidirectional flow assumption, the convection–diffusion equation for the ligand in the bulk is given by

$$\frac{\partial\tilde{C}}{\partial\tilde{t}}=D\left(\frac{\partial^2\tilde{C}}{\partial\tilde{x}^2}+\frac{\partial^2\tilde{C}}{\partial\tilde{y}^2}+\frac{\partial^2\tilde{C}}{\partial\tilde{z}^2}\right)-\tilde{v}(\tilde{y},\tilde{z})\frac{\partial\tilde{C}}{\partial\tilde{x}}, \tag{2.5}$$

where D is the molecular diffusion coefficient for the system. The scalings for $\tilde{v},\tilde{y}$, and $\tilde{z}$ have been given previously. For $\tilde{x}$, the proper scaling is the one associated with the reacting zones, which we treat as rectangles. We define the ijth reacting zone to be the one with $\tilde{x}\in[\tilde{x}_i^-,\tilde{x}_i^+],\tilde{z}\in\left[\tilde{z}_j^-,\tilde{z}_j^+\right]$, where $\tilde{x}_1^-=0$. We define the length of the first region as L_r, and consider the dimensions of each region to be of roughly that size. The reacting regions are separated by nonreacting regions of characteristic size L_n.

In general the convective time scale is much faster than the diffusive time scale. Hence in order to balance these effects, the flow region of interest is very near the reacting zones [20]. Thus we introduce a "floor layer" near $y_f=0$. So the proper scalings in the spatial directions are

$$x=\frac{\tilde{x}}{L_r},\quad y=\mathrm{Pe}^{1/3}y_f=\frac{\mathrm{Pe}^{1/3}\tilde{y}}{H}, \tag{2.6a}$$

where Pe is the Péclet number:

$$\mathrm{Pe}=\frac{\text{characteristic diffusion time}}{\text{characteristic convection time across the reacting surface}}=\frac{H^2/D}{L_r/V}. \tag{2.6b}$$

Note that with these scalings, $x_1^+=1$.

To choose a scale for $\tilde{C}$, we note that an ideal experiment would follow the well-mixed approximation without depletion due to

infinitely fast replenishment of ligand ($V = \infty$). Therefore, it is experimentally desirable to reduce the size of depletion as much as possible. Hence we introduce a scaling to make the dimensionless C into a deviation from the uniform initial value C_u. Since we are interested in tracking the reaction, we normalize $\tilde{t}$ by the forward reaction time scale. Hence these scalings become

$$\widetilde{C}(\tilde{x},\tilde{y},\tilde{z},\tilde{t}) = C_u[1 - \mathrm{Da}C(x,y,z_f,t)], \quad t = k_{on}C_u\tilde{t}, \tag{2.7}$$

where k_{on} is the forward rate constant for the reaction. Da is the Damköhler number, to be defined later. With this scaling, it is clear that in order to minimize the effects of depletion and transport, one wishes to make Da as small as possible. Fortunately, this is experimentally realizable.

Substituting (2.6a) and (2.7) into (2.5), we obtain

$$\kappa\frac{\partial C}{\partial t} = \frac{H^2}{L_r^2}\mathrm{Pe}^{-2/3}\frac{\partial^2 C}{\partial x^2} + \frac{\partial^2 C}{\partial y^2} + \epsilon^2\mathrm{Pe}^{-2/3}\frac{\partial^2 C}{\partial z_f^2} - \mathrm{Pe}^{1/3}v_f(\mathrm{Pe}^{-1/3}y, z_f)\frac{\partial C}{\partial x}, \tag{2.8a}$$

$$\kappa = \frac{\text{convective time scale in layer}}{\text{reaction time scale}} = \frac{L_r\mathrm{Pe}^{1/3}/V}{(k_{on}C_u)^{-1}}, \tag{2.8b}$$

where we have used (2.3), (2.4) and (2.6b). We note from the Appendix that $H/L_r = O(1)$ and $\mathrm{Pe} \gg 1$, so we may neglect the first term on the right-hand side of (2.8a). In addition, we have from the Appendix that $\kappa \ll 1$, so the left-hand side may be neglected as well, and we obtain

$$\frac{\partial^2 C}{\partial y^2} + \epsilon^2\mathrm{Pe}^{-2/3}\frac{\partial^2 C}{\partial z_f^2} = \mathrm{Pe}^{1/3}v_f(\mathrm{Pe}^{-1/3}y, z_f)\frac{\partial C}{\partial x}. \tag{2.9}$$

Because v_f must satisfy the no-slip condition at $z_f = 0$, we expect it to be linear in the boundary layer, which forces the last term to be $O(1)$. However, without an explicit form for v_f, it is not yet clear which of the terms in (2.9) form a dominant balance. Hence we delay further simplifications of (2.9) until later.

Since (2.9) is in steady state, no initial condition may be imposed. The physical reason for this is that with $\kappa \to 0$, transport is much faster than the reaction, so the flow in the layer has equilibrated before the transport begins. Hence the only change to the ligand concentration will come from coupling to the reaction zone.

Since y is a boundary-layer variable, the solution must obey the far-field condition

$$C(x,\infty,z_f,t) = 0, \tag{2.10a}$$

since the bulk flow is unaffected by the reaction. Similarly, the reaction has not yet happened at the inflow, so

$$C(0,y,z_f,t) = 0. \tag{2.10b}$$

2.3. Kinetic equation

Since the only difference between our model for the Flexchip and the model in [23] for the 1-zone BIAcore is the number of reacting zones, the kinetic equation for $\widetilde{B}$, the (area) concentration of bound receptors, is the same as in that work:

$$\frac{\partial\widetilde{B}}{\partial\tilde{t}} = k_{on}(R - \widetilde{B})\widetilde{C}(\tilde{x},0,\tilde{z},\tilde{t}) - k_{off}\widetilde{B}, \quad (\tilde{x},\tilde{z}) \in \partial\mathcal{R}_r, \tag{2.11}$$

where k_{off} is the backward rate constant for the reaction. Hence we follow the analysis in [23]. The only substantive difference here is that (2.11) holds only in the portion of the floor containing the reacting zones, which we denote as $\partial\mathcal{R}_r$. We then normalize $\widetilde{B}$ by the (uniform) concentration of empty receptors R at the beginning of the experiment:

$$B(x,z_f,t) = \frac{\widetilde{B}(\tilde{x},\tilde{z},\tilde{t})}{R}. \tag{2.12}$$

Substituting (2.7) and (2.12) into (2.11), we obtain

$$\frac{\partial B}{\partial t} = (1 - B)[1 - \mathrm{Da}C(x,0,z_f,t)] - KB, \quad (x,z_f) \in \partial\mathcal{R}_r, \tag{2.13a}$$

$$K = \frac{k_{off}}{k_{on}C_u}. \tag{2.13b}$$

Here K is a normalized affinity constant.

The (diffusive) flux into the reacting surface must be used up in the reaction, so we have

$$D\frac{\partial\widetilde{C}}{\partial\tilde{y}}(\tilde{x},0,\tilde{z},\tilde{t}) = \frac{\partial\widetilde{B}}{\partial\tilde{t}}, \quad (\tilde{x},\tilde{z}) \in \partial\mathcal{R}_r. \tag{2.14}$$

Substituting (2.6a), (2.7) and (2.12) into (2.14), we obtain the following:

$$\frac{\partial C}{\partial y}(x,0,z_f,t) = -\frac{\partial B}{\partial t}I(x,z_f), \quad I(x,z_f) = \begin{cases} 1, & (x,z_f) \in \partial\mathcal{R}_r, \\ 0, & (x,z_f) \in \partial\mathcal{R}_n, \end{cases} \tag{2.15a}$$

$$\mathrm{Da} = \frac{k_{on}R}{D/(H\mathrm{Pe}^{-1/3})} = \frac{\text{reaction "velocity"}}{\text{diffusion "velocity" in diffusive boundary layer}}, \tag{2.15b}$$

where we have used the fact that there is no flux through the nonreacting zone $\mathcal{R}_n$.

The Flexchip measures the average of the bound state within each reacting zone, returning the result as a *sensogram signal*, which depends only on t. Hence we define $\mathcal{S}_{ij}$, the average sensogram signal from the ijth reacting zone, as

$$\mathcal{S}_{ij}[B] = \frac{1}{(x_i^+ - x_i^-)(z_j^+ - z_j^-)}\int_{z_j^-}^{z_j^+}\int_{x_i^-}^{x_i^+} B(x,z_f,t)\,dx\,dz_f. \tag{2.16}$$

A biosensor experiment normally consists of two parts. In an *association experiment* the receptors in the reacting zones are empty, and (as discussed previously) ligand flows from the left with input value C_u. Hence the initial condition for B in an association experiment is given by

$$B(x,z_f,0) = 0. \tag{2.17}$$

2.4. Dissociation experiments

After the association experiment has run to steady state, one starts a *dissociation experiment* by shutting off the ligand supply and allowing the bound state to dissociate over time. Hence the initial condition for a dissociation experiment is the steady state B_s of the association experiment. The steady state of (2.15a) implies that the ligand concentration is uniform in y, which means that $C = 0$ to match the far-field condition (2.10a). Substituting this result into (2.13a) yields

$$B_s \equiv \frac{1}{\alpha}, \quad \alpha = 1 + K, \tag{2.18a}$$

and hence

$$B(x,z_f,0) = \alpha^{-1} \tag{2.18b}$$

is the initial condition for B for a dissociation experiment.

During the dissocation experiment, there is no ligand flowing into the channel. However, since B_s (and hence the initial condition

(2.18b)) depends on C_u (through α), we keep the same size scaling as in (2.7), simply replacing it by

$$\tilde{C}(\tilde{x},\tilde{y},\tilde{t}) = C_u \mathrm{Da} C(x,y,t). \tag{2.19}$$

Replacing (2.7) with (2.19) yields the following equations, analogous to (2.13a) and (2.15a):

$$\frac{\partial B}{\partial t} = (1-B)\mathrm{Da}C(x,0,t) - KB, \quad (x,z_f) \in \partial\mathcal{R}_r, \tag{2.20a}$$

$$\frac{\partial C}{\partial y}(x,0,t) = \frac{\partial B}{\partial t} I(x,z_f). \tag{2.20b}$$

Note that the new scaling will not affect (2.9).

3. Outer solution (depletion effects)

In order to solve the problem, we first consider the flow field. Motivated by the Appendix, we use the fact that $\epsilon \ll 1$ in (2.4) to yield

$$v_f(y_f,z_f) = y_f(1-y_f), \tag{3.1}$$

which is exactly the expression we obtain if ignoring the walls entirely [23]. Indeed, this solution will break down only for distances $z_f = O(\epsilon)$ from the walls, which corresponds to $\tilde{z} = O(H)$. Therefore, as long as the spots are far enough away from the outer walls, the effect of their presence may be ignored. (We will explicitly quantify "far enough", which turns out to be much closer than $O(H)$, in the next section.)

In the floor layer where $y_f \to 0$, we have from (3.1) that

$$v_f(y_f,z_f) \sim y_f = \mathrm{Pe}^{-1/3} y. \tag{3.2}$$

Substituting (3.2) into (2.9), we obtain the following:

$$\frac{\partial^2 C}{\partial y^2} = y\frac{\partial C}{\partial x}. \tag{3.3}$$

Also, with this approximation, any contributions to the flux from the boundary layers will be negligible. Hence we can relate V to the flow rate Q as follows:

$$Q = \int_0^H \int_0^W \tilde{v}(\tilde{y},\tilde{z})\,d\tilde{z}\,d\tilde{y} = \frac{VWH}{6}. \tag{3.4}$$

Note that by using (3.4) and (2.6b) in (2.15b), we may obtain an expression for Da in terms of Q:

$$\mathrm{Da} = k_{on} R \left(\frac{WH^2 L_r}{6QD^2}\right)^{1/3}. \tag{3.5}$$

Hence increasing the flow rate decreases Da (and hence the effect of transport), as expected.

3.1. Association experiment

Since there is no explicit z_f-dependence in (3.3), C is independent of z_f away from the walls (since the influx condition is), and so is B. We may solve (3.3) subject to the boundary and matching conditions (2.10) via Laplace transforms in x. (We may take x to be semi-infinite without difficulty because of the placement of the reacting zones [23].)

The result in Laplace transform space is an Airy function, whose value at $y = 0$ must be known in order to obtain the quantity $C(x,0,t)$, which is the only fact we need in (2.13a). The Laplace transform of this quantity can be expressed in terms of its y-derivative, and the entire expression inverted to yield

$$\begin{aligned} C(x,0,t) &= -\frac{1}{3^{1/3}\Gamma(2/3)} \int_0^x \frac{\partial C}{\partial y}(\xi,0,t) \frac{d\xi}{(x-\xi)^{2/3}} \\ &= \frac{1}{3^{1/3}\Gamma(2/3)} \int_0^x \frac{\partial B}{\partial t}(\xi,t) I(\xi) \frac{d\xi}{(x-\xi)^{2/3}}, \end{aligned} \tag{3.6}$$

where in the last line we have used (2.15a). If there is only a single reacting zone, $I(\xi) \equiv 1$ and we reduce to the case of a single reacting zone in the BIAcore [24]. Note that the integral in (3.6) has a clear physical interpretation: namely that C is influenced by depletion effects upstream (which occur only in the regions where $I(\xi) = 1$).

Also note that the influence of $\partial B/\partial t$ decays with distance away from x. Therefore, even though there is no ligand being drawn out of the system in the nonreacting zones, the concentration is still affected because of this decaying "memory effect". In physical terms, (3.3) is a balance between convection in the x-direction and diffusion in the y-direction. Hence ligand has a chance to diffuse back to the surface in the absence of the driving force of the reaction.

As mentioned above, to minimize transport effects scientists design experiments so $\mathrm{Da} \ll 1$. Hence we expand B in a perturbation series in Da:

$$B(x,t) = B_0(x,t) + \mathrm{Da}B_1(x,t) + o(\mathrm{Da}). \tag{3.7}$$

Substituting (3.7) into (2.13a) and (2.17) and solving, we obtain, to leading order,

$$B_0(x,t) = \frac{1-e^{-\alpha t}}{\alpha}. \tag{3.8}$$

We plot B_0 in Fig. 3 using the parameters in Table 1. Here the parameters are chosen as representative values from the ranges shown in the Appendix. Note also that by choosing a fixed value of k_{on} to set the time scale, the variance of K in Fig. 3 is set solely by varying k_{off}. Varying K (and hence α) changes not only the steady state, but also the characteristic time of the evolution, consistent with (3.8).

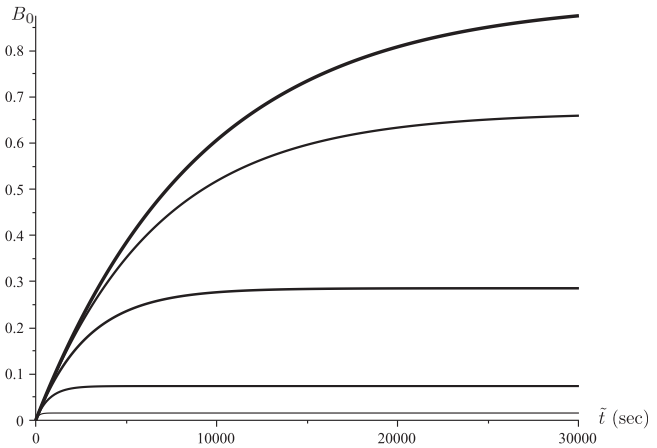

Fig. 3. Concentration of the bound state, normalized by initial receptor site density (B_0 as given in (3.8)) *vs.* $\tilde{t}$ for (in decreasing order of thickness) $K = 0.1, 0.5, 2.5, 12.5, 62.5$.

Table 1
Parameter values for computations.

Parameter	Value	Parameter	Value
C_u (mol/cm^3)	10^{-11}	t	$10^{-4}\tilde{t}$/s
k_{on} (cm^3/mol/s)	10^7		

Since Da = 0 in the leading-order solution, (3.8) is the solution in the well-mixed case, and hence is spatially uniform. Thus to leading order we may pull the $\partial B/\partial t$ term out of the integrand in (3.6), leaving a simple integral we can compute:

$$C(x,0,t) = \frac{1}{3^{1/3}\Gamma(2/3)}\frac{dB_0}{dt}\int_0^x I(\xi)\frac{d\xi}{(x-\xi)^{2/3}} + O(\mathrm{Da}) = \frac{dB_0}{dt}h_\infty(x) + O(\mathrm{Da}), \tag{3.9}$$

$$h_\infty(x) = \frac{3^{2/3}x^{1/3}}{\Gamma(2/3)}, \quad x \in [0,1], \tag{3.10a}$$

$$h_\infty(x) = \frac{3^{2/3}}{\Gamma(2/3)}\left\{\sum_{n=1}^{i-1}\left[(x-x_n^-)^{1/3} - (x-x_n^+)^{1/3}\right] + (x-x_i^-)^{1/3}\right\}, \quad x \in [x_i^-, x_i^+], \quad i > 1, \tag{3.10b}$$

where the ∞ notation will become clear in the next section. Substituting (3.7) and (3.9) into (2.13a), we obtain

$$\frac{\partial B}{\partial t} + \mathrm{Da}(1-B_0)\frac{dB_0}{dt}h_\infty = 1 - \alpha B + O(\mathrm{Da}^2). \tag{3.11}$$

In order to analyze the experimental data, expressions for B are not enough: we must translate them into expressions for the sensogram signal. Since B is independent of z_f, we may average (2.16) immediately in that direction to obtain

$$\mathcal{S}_i[B] = \frac{1}{x_i^+ - x_i^-}\int_{x_i^-}^{x_i^+} B(x,t)\,dx \tag{3.12}$$

for any zone in the ith row.

Using (3.12) to rewrite (3.11) in terms of the signal, we obtain

$$\frac{d\mathcal{S}_i[B]}{dt} + \mathrm{Da}_i(1-\mathcal{S}_i[B_0])\frac{d\mathcal{S}_i[B_0]}{dt} = 1 - \alpha\mathcal{S}_i[B] + O(\mathrm{Da}^2), \quad \mathrm{Da}_i = \mathrm{Da}\mathcal{S}_i[h_\infty]. \tag{3.13}$$

Here Da_i is an effective Damköhler number that now incorporates the position of the reacting zone along the channel. Since $B = B_0 + O(\mathrm{Da})$, we may simplify (3.13) to obtain

$$\frac{d\mathcal{S}_i[B]}{dt} = \frac{1-\alpha\mathcal{S}_i[B]}{1+\mathrm{Da}_i(1-\mathcal{S}_i[B])} + O(\mathrm{Da}^2), \quad \mathcal{S}_i[B](0) = 0, \tag{3.14}$$

where we have derived the initial condition by averaging (2.17).

A complete model for the Flexchip would be the PDE system involving (3.3) or the nonlinear integrodifferential equation that would result upon substituting (3.6) into (2.13a). However, in the limit of small Da, we may effectively approximate the sensogram signal by the solution of the simple ODE (3.14), which is much easier to solve numerically through device software. For this reason, we denote (3.14) as an *effective rate constant* (ERC) equation.

For completeness, we compute the general expressions for Da_i, which are as follows:

$$\mathrm{Da}_1 = \frac{3^{5/3}\mathrm{Da}}{4\Gamma(2/3)}, \tag{3.15a}$$

$$\mathrm{Da}_i = \frac{\mathrm{Da}_1}{x_i^+ - x_i^-}\left\{(x_i^+ - x_i^-)^{4/3} + \sum_{n=1}^{i-1}\left[(x_i^+ - x_n^-)^{4/3} - (x_i^+ - x_n^+)^{4/3} - (x_i^- - x_n^-)^{4/3} + (x_i^- - x_n^+)^{4/3}\right]\right\}, \quad i > 1. \tag{3.15b}$$

However, in order to plot results, we specialize to the case of the Flexchip described in [15]. In that paper, the width of the reacting zones and the nonreacting zones are all equal (and with our scalings are normalized to 1), so we have $x_i^- = 2(i-1)$, $x_i^+ = 2i-1$. Exploiting these simpler expressions as well as cancellation properties of the sum, we obtain

$$\mathrm{Da}_i = \mathrm{Da}_1\left[(2i-1)^{4/3} + 2\sum_{n=1}^{2i-2}(-1)^{n+1}n^{4/3}\right], \tag{3.16a}$$

which can be written recursively as

$$\mathrm{Da}_{i+1} = \mathrm{Da}_i + \mathrm{Da}_1\left[(2i-1)^{4/3} - 2(2i)^{4/3} + (2i+1)^{4/3}\right]. \tag{3.16b}$$

As zones are placed further downstream, i increases. Upon noting that the bracketed expression is related to a difference approximation to the (positive) second derivative of $x^{4/3}$, it is clear that Da_i (and hence the effect of depletion) increases as the zones are placed further downstream.

From the form of (3.15b), we see that the effect of zone placement is simply to change the coefficient in front of the experimental parameter Da. The effect of varying Da on the bound-state evolution has been well-documented (cf. [20,23,25,26]), and so in this work we pick a single value of Da and consider only the effects of zone placement.

In Fig. 4 we plot the difference between the solution of the ERC equation and the well-mixed solution B_0 for various values of i. We use the parameters in Table 1, the Flexchip model that yielded (3.16a), and the following additional parameter values:

$$K = 1, \quad \mathrm{Da} = 0.1, \tag{3.17}$$

which are within the ranges in the Appendix. The quantity plotted is $B_0 - \mathcal{S}_i[B] > 0$, so the transport effects slow the pace of the reaction. As shown in the inset, rather than creating a "bump" or "dimple" in the sensogram data, depletion simply slows its rise, causing a naïve user to underestimate the true rate constant.

Also, note that as i increases, the transport effect increases, as predicted. However, the small size of Da (both mathematically necessary for the analysis and experimentally desirable) ensures that the depletion difference between the zone with $i = 1$ and downstream zones is quite small. This small variation in the data between reacting zones has been seen in the literature (cf. [15,27,28]).

3.2. Dissociation experiment

Since the scaling (2.19) in a dissociation experiment does not affect (2.9), (3.3) also holds. Since the only difference between (2.15a) and (2.20b) is a minus sign, (3.6) becomes

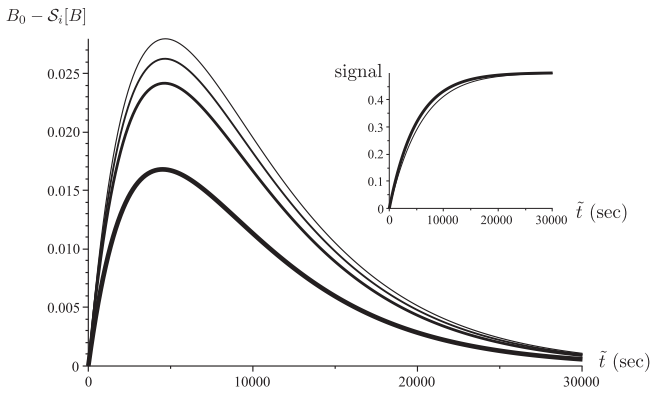

Fig. 4. Difference between well-mixed normalized bound state solution (3.8) and the solution to the ERC Eq. (3.14), which incorporates transport effects. In decreasing order of thickness: $i = 1$ (1-zone BIAcore), 2, 3, 4, 5. Inset: B_0 (thick line) and $\mathcal{S}_5[B]$ (thin line).

$$C(x,0,t) = -\frac{1}{3^{1/3}\Gamma(2/3)}\int_0^x \frac{\partial B}{\partial t}(\xi,t)I(\xi)\frac{d\xi}{(x-\xi)^{2/3}}. \tag{3.18}$$

Substituting (3.7) into (2.20a) and (2.18b), we obtain, to leading order,

$$B_0(x,t) = \frac{e^{-\alpha t}}{\alpha}. \tag{3.19}$$

We again have a simple spatially uniform exponential analogous to (3.8) in the association case. The solution is plotted in Fig. 5 using the same parameters as before. Again note that increasing K reduces both the initial condition (which is the steady state of the association experiment) and the characteristic time scale.

Since the solution for B_0 is spatially uniform, we may rewrite (3.18) as

$$C(x,0,t) = -\frac{dB_0}{dt}h_\infty(x) + O(\mathrm{Da}), \tag{3.20}$$

where $h_\infty(x)$ is as defined in (3.10). Substituting (3.7) and (3.20) into (2.20a), we obtain

$$\frac{\partial B}{\partial t} + \mathrm{Da}(1-B_0)\frac{dB_0}{dt}h_\infty = -KB + O(\mathrm{Da}^2),$$

which is the same as (3.11) with $1-\alpha B$ replaced by $-KB$. Hence (3.14) becomes

$$\frac{d\mathcal{S}_i[B]}{dt} = \frac{-K\mathcal{S}_i[B]}{1+\mathrm{Da}_i(1-\mathcal{S}_i[B])} + O(\mathrm{Da}^2), \quad \mathcal{S}_i[B](0) = \alpha^{-1}, \tag{3.21}$$

where Da_i is defined in (3.15b).

Fig. 6 is the dissociation analog to Fig. 4. In this case $B_0 - \mathcal{S}_i[B] < 0$. So dissociation goes faster when $\mathrm{Da} = 0$, and the transport effects slow the pace of the reaction. Again the size of the depletion effect moving downstream is small.

4. Inner solution (wall effects)

Obviously the solution (3.1) for the flow does not satisfy the no-slip conditions on the walls $z_f = 0$, $z_f = 1$. Since in the Flexchip multiple reacting zones are aligned along the channel width, we must consider changes in the flow now near the walls to determine whether they will affect our experimental results.

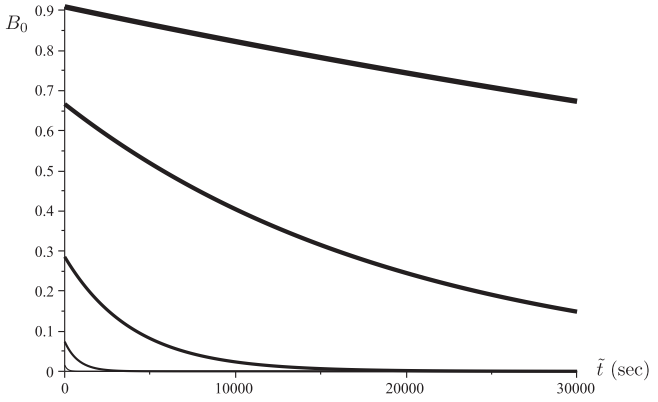

Fig. 5. Concentration of the bound state, normalized by initial receptor site density (B_0 as given in (3.19)) *vs.* $\tilde{t}$ for (in decreasing order of thickness) $K = 0.1, 0.5, 2.5, 12.5, 62.5$.

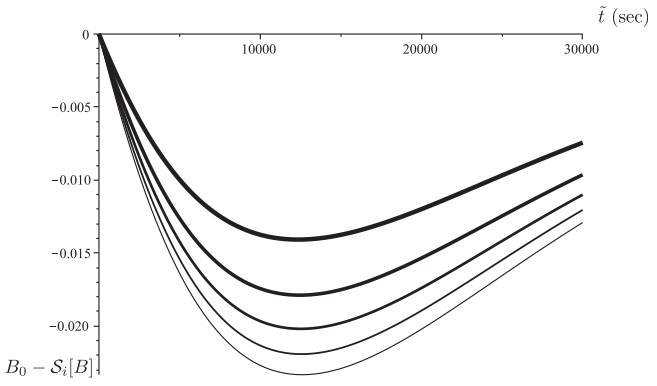

Fig. 6. Difference between well-mixed normalized bound state solution (3.19) and the solution to the ERC Eq. (3.21), which incorporates transport effects. In decreasing order of thickness: $i = 1$ (1-zone BIAcore), 2, 3, 4, 5.

Due to the underlying symmetry of the problem, it is sufficient to solve only near $z_f = 0$ by defining the following "wall-layer" variable:

$$z = \frac{z_f}{\epsilon}. \tag{4.1a}$$

Since we are interested in the deviation from the outer solution due to wall effects, we scale the velocity in that fashion:

$$v_f(y_f,z_f) = y_f(1-y_f) - v(y_f,z), \quad z_f \to 0, \tag{4.1b}$$

where we have used (3.1). Note our formulation in (4.1b) indicates that v is the deviation of the velocity in the wall layer from the undisturbed outer solution.

Substituting (4.1) into (2.4), we obtain

$$\frac{\partial^2 v}{\partial y_f^2} + \frac{\partial^2 v}{\partial z^2} = 0. \tag{4.2}$$

The solution to this PDE must satisfy all three no-slip conditions:

$$v(0,z) = v(1,z) = 0, \quad v(y_f,0) = y_f(1-y_f), \tag{4.3a}$$

where the third condition arises from the form of (4.1b). Also given this form, the matching condition becomes

$$v(y_f,\infty) = 0, \tag{4.3b}$$

since as we exit the layer the deviation must go to zero.

The form of the y_f boundary conditions in (4.3a) motivates a sine-series solution. Rewriting (4.2) and (4.3) in transform space and solving, we obtain the following solution for v_f:

$$v_f(y_f,z_f) = y_f(1-y_f) - \sum_{n=0}^{\infty}\frac{8}{(2n+1)^3\pi^3}\exp(-(2n+1)\pi z) \times \sin(2n+1)\pi y_f, \tag{4.4}$$

which in general is difficult to analyze. However, to examine the ligand transport Eq. (2.9) we need only the behavior of the function in the floor layer near $y_f = 0$. Hence we have

$$v_f(y_f,z_f) \sim y_f[1 - v_\Delta(z)], \quad y_f \to 0, \quad z_f \to 0, \tag{4.5a}$$

$$v_\Delta(z) = \sum_{n=0}^{\infty}\frac{8}{(2n+1)^2\pi^2}\exp(-(2n+1)\pi z). \tag{4.5b}$$

With (4.5a) replacing (3.2), (2.9) becomes

$$\frac{\partial^2 C}{\partial y^2} = y[1 - v_\Delta(z)]\frac{\partial C}{\partial x}, \tag{4.6}$$

where we have used the fact that $\mathrm{Pe} \gg 1$ to eliminate the z-derivative terms. But since z does not appear in the derivatives, we can

transform (4.6) into (3.3) by letting $y' = y[1 - v_\Delta(z)]^{1/3}$. Hence (3.6) becomes

$$C(x,0,z,t) = -\frac{1}{3^{1/3}\Gamma(2/3)[1-v_\Delta(z)]^{1/3}}\int_0^x \frac{\partial C}{\partial y}(\xi,0,z,t)\frac{d\xi}{(x-\xi)^{2/3}} = \frac{1}{3^{1/3}\Gamma(2/3)[1-v_\Delta(z)]^{1/3}}\int_0^x \frac{\partial B}{\partial t}(\xi,z,t)I(\xi)\frac{d\xi}{(x-\xi)^{2/3}} \tag{4.7}$$

and the effect of the wall simply appears as a factor premultiplying our previous work.

When Da is small, B_0 is still a function of t only and we obtain

$$C(x,0,z,t) = \frac{dB_0}{dt}h(x,z) + O(\mathrm{Da}), \quad h(x,z) = \frac{h_\infty(x)}{[1-v_\Delta(z)]^{1/3}}, \tag{4.8}$$

where $h_\infty(x) = h(x,\infty)$ is defined in (10). Note that as in [29], the contributions from transport in the various directions decouple.

But note from (4.5a) that as $z \to 0$, $1 - v_\Delta(z) \to 0$ to satisfy the no-slip condition, and hence $C \to \infty$. To explain the paradox, recall that C is the scaled displacement from the inlet value. In most of the channel, when the reaction occurs (driving the concentration down and C up), there is a velocity field that convects new ligand to the receptor sites, reversing that process. However as $z \to 0$, there is no velocity field by (4.6), so (in this scaling) the depletion continues *ad infinitum*, driving C to infinity.

Hence our scaling must fail as $z \to 0$. In particular, as $z \to 0$, C is eventually going to become $O(\mathrm{Da}^{-1})$, which would then violate the assumptions that lead to (4.8). In this case, the true ligand concentration $1 - \mathrm{Da}C$ would go to zero at the reacting zone, driving $\partial B/\partial t$ to zero and making (4.7) well-behaved. Thus in order for (4.8) to be valid, we must have

$$[1 - v_\Delta(z)]^{1/3} \gg \mathrm{Da}. \tag{4.9}$$

To calculate a value of z corresponding to this bound, we first obtain a simpler expression for v_Δ by noting that

$$v_\Delta'' = \frac{8e^{-\pi z}}{1-e^{-2\pi z}}, \quad v_\Delta'(\infty) = 0, \quad v_\Delta(\infty) = 0,$$

the solution of which is given by

$$v_\Delta(z) = \frac{4}{\pi^2}[\mathrm{dilog}(1-e^{-\pi z}) - \mathrm{dilog}(1+e^{-\pi z})], \tag{4.10}$$

where dilog is the dilogarithm function defined by [30]

$$\mathrm{dilog}\,\xi = \int_1^\xi \frac{\log \xi'}{1-\xi'}d\xi'. \tag{4.11}$$

This can also be determined directly from the sum in (4.5b) ([31], 27.7.2).

Expanding (4.10) for small z, we have that

$$1 - v_\Delta(z) \sim -\frac{4z\log z}{\pi} \gg \mathrm{Da}^3. \tag{4.12}$$

For the value of Da in (3.17), this yields

$$z \gg 8.4 \times 10^{-5}. \tag{4.13}$$

In the Flexchip, the distance between a zone and the wall is on the same order as the width of a zone, which we denote as Δz. Hence using the lower bound on Δz from the Appendix, we see that (4.13) is always satisfied.

Eq. (4.13) is a much less restrictive bound than the simple $O(H)$ bound mentioned at the beginning of Section 3. That is because the wall layer has a much larger effect on the core flow (where it drives an $O(1)$ velocity to zero) than it does on the floor layer (where the velocity is already $O(\mathrm{Pe}^{-1/3})$ to begin with).

To examine the effect of the distance from the wall on the sensogram signal, it is convenient to redefine the z-range of the reacting zone as $z \in [z_j, z_j + \Delta z]$. Hence we have that

$$\mathcal{S}_{ij}[B] = \frac{1}{(x_i^+ - x_i^-)\Delta z}\int_{z_j}^{z_j+\Delta z}\int_{x_i^-}^{x_i^+} B(x,z,t)dx\,dz. \tag{4.14}$$

To complete the solution, we see from (3.13) that we need the new value of $\mathrm{Da}\mathcal{S}_{ij}[h]$. Since the x- and z-dependences separate, the two integrals decouple and we obtain

$$\mathrm{Da}\mathcal{S}_{ij}[h] = \mathrm{Da}_i\beta(z_j), \quad \beta(z_j) = \frac{1}{\Delta z}\int_{z_j}^{z_j+\Delta z}\frac{1}{[1-v_\Delta(z)]^{1/3}}dz, \tag{4.15}$$

where we have used (3.13). To understand the physical meaning of β, we examine (4.8). Considering the concentration deviation C, we see that the ratio between the case including and ignoring the walls is given by

$$\frac{C(x,0,z,t)}{C(x,0,\infty,t)} = \frac{h(x,z)}{h_\infty(x)} = \frac{1}{[1-v_\Delta(z)]^{1/3}}. \tag{4.16}$$

Hence by (4.16) we see that β is just the average of this ratio over the jth spot. β hence quantifies how the bulk concentration (and hence the concentration of the bound state) is affected by the changes in flow velocity that occur near the wall. Therefore values of β near 1 correspond to zone placement where wall effects are negligible.

Note that the integral must be done numerically for each set of endpoints, but once computed for one zone, it can be stored and need not be recalculated. Since the x- and z-effects separate, it is sufficient to pick a particular i (we select $i = 1$) and then graph the relative effects of varying the z-position of the reacting zone.

Fig. 7 shows a graph of β *vs.* $\tilde{z}$ for the upper and lower bounds on Δz given in the Appendix. Note that it very quickly approaches the matching value 1, so in general we do not expect significant wall effects. In particular, if as described in [15], a 1 cm array of zones is centered in a 1.3 cm channel, then the closest reacting zone starts at $\tilde{z} = 0.15$ cm, which is outside the range of Fig. 7. So we expect wall effects to be negligible.

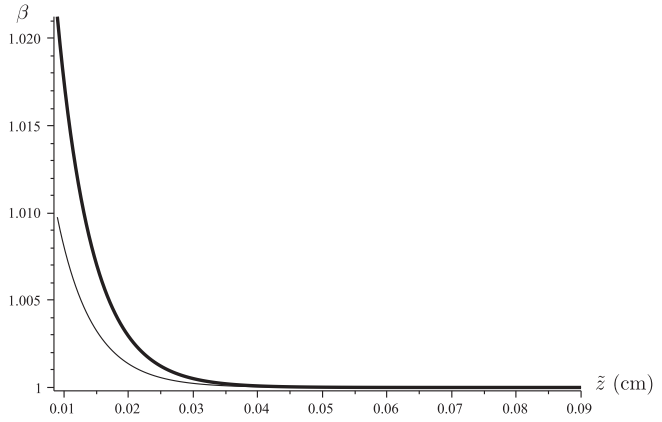

Fig. 7. Average concentration depletion across a reacting zone, normalized by the depletion infinitely far away from the wall, for $\Delta z = 8.33 \times 10^{-1}$ (thick line) and $\Delta z = 1.94$ (thin line). Here $\tilde{z}$ is measured as distance away from the wall.

With the computations in (4.15), we see that (3.14) and (3.21) become

$$\frac{d\mathcal{S}_{ij}[B]}{dt} = \frac{1-\alpha\mathcal{S}_{ij}[B]}{1+\mathrm{Da}_i\beta(z_j)(1-\mathcal{S}_{ij}[B])} + O(\mathrm{Da}^2), \quad \mathcal{S}_{ij}[B](0) = 0, \tag{4.17a}$$

$$\frac{d\mathcal{S}_{ij}[B]}{dt} = \frac{-K\mathcal{S}_{ij}[B]}{1+\mathrm{Da}_i\beta(z_j)(1-\mathcal{S}_{ij}[B])} + O(\mathrm{Da}^2), \quad \mathcal{S}_{ij}[B](0) = \alpha^{-1}. \tag{4.17b}$$

Fig. 8 shows the difference in the measured sensogram signal when one takes into account the z-placement of the layer. Note that the difference is exceedingly small.

These same arguments hold for the dissociation case, as shown in Fig. 9.

5. Remarks

5.1. The dotLab

The dotLab is another biosensor with multiple reacting zones. A schematic of the flow cell is shown in Fig. 10. (The optical principle used to take the measurements is different from that used in the Flexchip, but that is irrelevant to our analysis.).

As can be seen from the diagram, there are two major differences between the devices: the relative size of the reacting zones

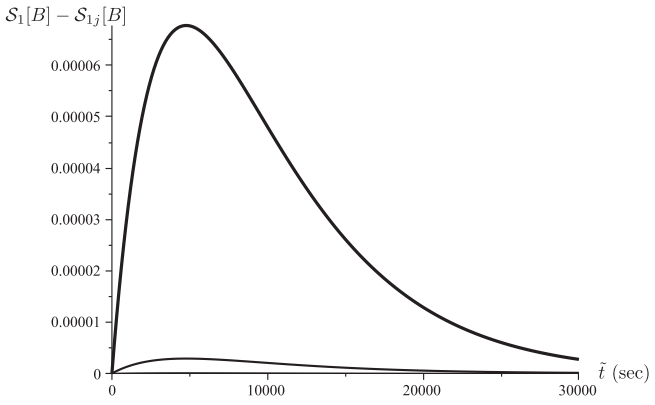

Fig. 8. Difference between the solution $\mathcal{S}_i[B]$ of (3.14) (which ignores wall effects) for the sensogram signal and the solution $\mathcal{S}_{ij}[B]$ of (4.17a). Here $i = 1$. In decreasing order of thickness: $z_j = 1, 2$.

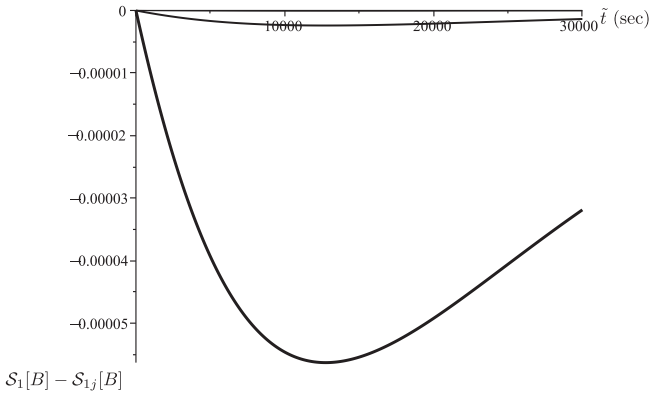

Fig. 9. Difference between the solution $\mathcal{S}_i[B]$ of (3.21) (which ignores wall effects) for the sensogram signal and the solution $\mathcal{S}_{ij}[B]$ of (4.17b). Here $i = 1$. In decreasing order of thickness: $z_j = 1, 2$.

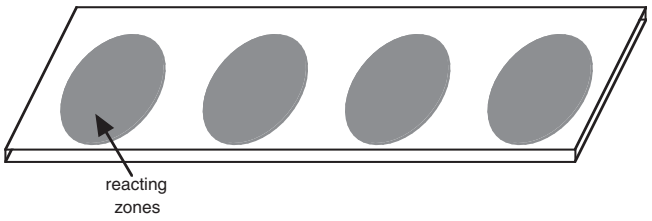

Fig. 10. Schematic of dotLab device.

as compared to the flow cell, and the number of columns of zones. Hence our discussion from Section 3 holds, and the difference between zones can be quantified through an effective Damköhler number. Also, from Section 4 we see that the placement of the zones in the $\tilde{z}$-direction is unimportant, so the position of the zone columns is irrelevant.

5.2. Generic flow fields

Given the geometry for the Flexchip indicated in Fig. 1, it is clear that we have made some simplifying assumptions when postulating unidirectional flow. Indeed, numerical simulations have shown [15] that the flow in the Flexchip can be quite complicated. Nevertheless, several aspects of our analysis are relevant to treatments of geometries and flow fields more similar to the actual device.

In particular, the differences we found in the x-direction were caused by depletion from upstream zones. Even in the context of more complicated flows, there will still be "upstream" and "downstream" zones, and the depletion effects will be similar. Fortunately, we found these effects to be small.

Moreover, it has been shown [26] that in the experimentally important case of small Da, the leading order B_0 of the bound state will always be spatially uniform, as in (3.8) and (3.19). Hence the time- and space-components of the deviation C from the upstream ligand concentration will decouple as in (4.8). For a different geometry or flow field, there will just be a different form for h, but the form (4.8) will still hold. As an added advantage, h is a function of only the flow field and geometry—parameters associated with the device, not the experiment. Hence h need be computed only once for a device, and its value stored for use in analyzing all reactions tested with that device.

6. Discussion

Many biological processes occur in surface-volume geometries. Because of the complicated structures involved, in many cases the surface contains multiple reacting zones for the same ligand. In order to devise an appropriate mathematical model for such systems, we begin by modeling optical biosensors with similar geometry and dynamics.

These biosensors with multiple reacting zones are designed to acquire data more quickly and efficiently. This data is then used to understand the underlying kinetics of both biological mechanisms and industrial processes. However, such data can be used for parameter estimation only with a proper mathematical model to interpret it.

In particular, given the imposed flow in such devices, depletion will reduce the amount of ligand available to bind to downstream zones. In addition, even though flow throughout most of the device (and hence most of the zones) is uniform in z, the flow field will be different near the channel sides, as it must transition from the bulk flow field to the no-slip condition at the wall. Hence it is reasonable to consider whether placing zones in these

areas will affect the measurements. In this paper we examined both possibilities.

In Section 2 we presented the general governing equations that hold under a uniform flow assumption. By exploiting its small aspect ratio, in Section 3 we established that in most of the channel, edge effects are negligible and the system can be treated as two-dimensional with reacting zones aligned in series. Hence the model is quite similar to that for the one-zone BIAcore device, with one key difference: namely, the ligand available for any row is reduced by depletion in the upstream rows.

In Section 4 we examined the boundary layers in the flow near the channel walls. In this region, the "core flow" away from the channel floor goes from $O(1)$ to zero at the wall. However, for the purposes of the reaction, the important region is not the core flow; rather it is the "unstirred layer" of width $O(\mathrm{Pe}^{-1/3})$ near $y = 0$. Using a separation-of-variables technique, we were able to separate the effects of transport in the x- and z-directions, as illustrated in (4.7), which differs from (3.6) only through a z-dependent premultiplier.

In the unstirred layer that is of interest, the velocity is $O(\mathrm{Pe}^{-1/3})$. Hence the adjustment in the velocity required to satisfy the no-slip condition at the wall is minimal. This is indicated by the bound (4.9), which is violated only for values of z so small that the reacting zones will never reach them.

6.1. Conclusions

When using an optical biosensor with multiple reacting zones, geometric considerations can be effectively decoupled into two categories: those concerned with placement along the channel length, and those concerned with placement across the channel width.

Our results show that placement along the channel length does have an effect on the bound state (cf. Figs. 4 and 6, which echo the experimental results in [15,27,28]). In particular, the reaction proceeds more slowly due to depletion of the ligand upstream. For the experimentally common case of small Da, these effects can be encapsulated in the effective Damköhler number Da_i as defined in (3.16). Zones placed further down the channel have increased i (and hence Da_i), which slows the reaction, as can be seen from Eq. (3.14) for the sensogram signal.

Our results show that placement across the channel width does not have an appreciable effect on the bound state (cf. Figs. 8 and 9). As shown in Fig. 7, the ligand concentration as close as 0.04 cm to the wall is the same as that in the center of the channel to within one part in a thousand. Therefore, designers may push the zones as close to the wall as practicable (allowing greater array density) without concern about introducing spurious measurement data.

These results have wider applicability beyond the Flexchip. Not only does the dotLab device have a similar geometry, but as discussed in Section 1, other biological and industrial applications exist in such unidirectional flow regimes. Moreover, due to the convenient structure of the ERC equation, the effect of the geometry manifests itself only through $h(x,z)$, which need be computed only once for each device.

6.2. Further research

In the context of modeling the Flexchip, several mathematical systems arise. The first, Eq. (2.4) for the velocity subject to inflow and non-slip conditions, has been well studied, However, the nonlinear system of boundary conditions (2.13a) and (3.6) makes the PDE system for C including (3.3) quite nonstandard. The focus of this manuscript has been constructing the model and solving it for parameters and boundary conditions specific to the Flexchip. We delay the interesting question of whether such a system is well-posed for all such conditions to later work.

Further research will focus on refining our work to model such biosensors more accurately. In particular, we shall relax the unidirectional flow assumption, consider different geometric array patterns, and model the effect of circular reacting zones.

Acknowledgments

The author thanks the referees for their detailed and insightful comments.

Appendix A

In Table 2 we list relevant parameter values for our analysis of the Flexchip, using product information about the BIAcore when possible [16] and referencing [15] when not. In [15], the reacting zones were considered to be circles with diameters equal to L_r and with closest spacing between the circles equal to L_n. The lower bound on L_n is from the simulation, while the upper bound comes from the calculations on Fig. 1A (both from [15]).

Table 3 shows the range of values for parameters used in this paper. Note that the velocity V is smaller than the typical range in the BIAcore [23] because of the larger cross-sectional area of the Flexchip channel. On the other hand, since we scale x by the length of the reacting zone, the minimum Pe is much larger than in the BIAcore [23]. The wide range of Da is typical for these systems, though the larger values are obtained only under extremely unlikely conditions.

When examining the full three-dimensional model for the Flexchip, one finds that the appropriate Reynolds number for the flow is

$$\mathrm{Re} = VH^2/\nu L_f. \tag{A.1}$$

The value in the table was calculated using $\nu = 10^{-2}$ cm^2/s, which is the kinematic viscosity of water at 20 °C [32]. Note that this value places the system well within the laminar regime.

Table 2
Parameter values from the literature.

Parameter	Value	Reference
C_u (mol/cm^3)	$2.98 \times 10^{-12} - 2 \times 10^{-10}$	[15]
D (cm^2/s)	6.94×10^{-6}	[15]
H (cm)	1.8×10^{-2}	[16]
k_{off} (s^{-1})	$10^{-5} - 10^{-2}$	[16]
k_{on} (cm^3 s/mol)	$10^5 - 10^9$	[16]
L_f (cm)	2	[15]
L_n (cm)	$2 \times 10^{-2} - 2.44 \times 10^{-2}$	[15]
L_r (cm)	$1.5 \times 10^{-2} - 3.5 \times 10^{-2}$	[16]
Q (μL/min)	100–1500	[16]
R (mol/cm^2)	$1.11 \times 10^{-13} - 2.33 \times 10^{-11}$	[15]
W (cm)	1.3	[15]

Table 3
Calculated parameter values.

Parameter	Value	Parameter	Value
Da	$1.06 \times 10^{-6} - 7.28$	V (cm/s)	$4.27 \times 10^{-1} - 6.41$
K	$5 \times 10^{-5} - 3.36 \times 10^{4}$	Δz	$8.33 \times 10^{-1} - 1.94$
Pe	$5.70 \times 10^{2} - 2.00 \times 10^{4}$	ϵ	1.38×10^{-2}
Re	$\leqslant 8.01 \times 10^{-1}$	κ	$1.89 \times 10^{-8} - 1.36 \times 10^{-1}$

References

[1] M. Raghavan, M.Y. Chen, L.N. Gastinel, P.J. Bjorkman, Investigation of the interaction between the class I MHC-related Fc receptor and its immunoglobulin G ligand, Immunity 1 (1994) 303.

[2] S. Mann, S.L. Burkett, S.A. Davis, C.E. Fowler, N.H. Mendelson, S.D. Sims, D. Walsh, N.T. Whilton, Sol-gel synthesis of organized matter, Chem. Mater. 9 (1997) 2300.

[3] H. Treml, S. Woelki, H.-H. Kohler, Theory of capillary formation in alginate gels, Chem. Phys. 3 (2003) 341.

[4] E.F. Grabowski, L.I. Friedman, E.F. Leonard, Effects of shear rate on the diffusion and adhesion of blood platelets to a foreign surface, Ind. Eng. Chem. Fund. 11 (1972) 224.

[5] B. Goldstein, M. Dembo, Approximating the effects of diffusion on reversible reactions at the cell surface: Ligand-receptor kinetics, Biophys. J. 68 (1995) 1222.

[6] S.R. Gundlapally, R. Agrawal, D.H. West, V. Balakotaiah, Influence of non-uniform activity and conductivity on stationary and moving patterns in catalytic reactors, Chem. Eng. Sci. 65 (5) (2010) 1522.

[7] S. Bhattacharyya, K.L. Warfield, G. Ruthel, S. Bavari, M.J. Aman, T.J. Hope, Ebola virus uses clathrin-mediated endocytosis as an entry pathway, Virology 401 (1) (2010) 18.

[8] B. Goldstein, C. Wofsy, H. Echavarría-Heras, Effect of membrane flow on the capture of receptors by coated pits, Biophys. J. 53 (1988) 405.

[9] A.J.C. Pommier, G. Alves, E. Viennois, S. Bernard, Y. Communal, B. Sion, G. Marceau, C. Damon, K. Mouzat, F. Caira, S. Baron, J.M.A. Lobaccaro, Liver X receptor activation downregulates AKT survival signaling in lipid rafts and induces apoptosis of prostate cancer cells, Oncogene 29 (18) (2010) 2712.

[10] R.L. Rich, D.G. Myszka, Survey of the year 2007 commercial optical biosensor literature, J. Mol. Recognit. 21 (2008) 355.

[11] R.L. Rich, D.G. Myszka, Grading the commercial optical biosensor literature—Class of 2008: 'The mighty binders'. J. Mol. Recognit. 23 (2010) 1.

[12] P.B. Garland, Optical evanescent wave methods for the study of biomolecular reactions, Quart. Rev. Biophys. 29 (1996) 91.

[13] J.-F. Houle, A novel approach to label-free sensing: diffractive optics technology (dot®), Comb. Chem. High Throughput Screen. 12 (2009) 801.

[14] A. Szabo, L. Stolz, R. Granzow, Surface plasmon resonance and its use in biomolecular interaction analysis (BIA), Curr. Opin. Struct. Bio. 5 (1995) 699.

[15] R.L. Rich, M.J. Cannon, J. Jenkins, P. Pandian, S. Sundaram, R. Magyar, J. Brockman, J. Lambert, D.G. Myszka, Extracting kinetic rate constants from surface plasmon resonance array systems, Anal. Biochem. 373 (1) (2008) 112.

[16] GE Healthcare, Uppsala, Biacore Flexchip Product Information, 2006.

[17] R.L. Rich, D.G. Myszka, Higher-throughput, label-free, real-time molecular interaction analysis, Anal. Biochem. 361 (1) (2007) 1.

[18] L.L.H. Christensen, Theoretical analysis of protein concentration determination using biosensor technology under conditions of partial mass transport limitation, Anal. Biochem. 249 (1997) 153.

[19] D.A. Edwards, Steric hindrance effects in thin reaction zones: applications to BIAcore, IMA J. Appl. Math. 72 (2007) 865.

[20] D.A. Edwards, B. Goldstein, D.S. Cohen, Transport effects on surface-volume biological reactions, J. Math. Bio. 39 (1999) 533.

[21] D.G. Myszka, X. He, M. Dembo, T.A. Morton, B. Goldstein, Extending the range of rate constants available from biacore: interpreting mass transport influenced binding data, Biophys. J. 75 (1998) 583.

[22] L.G. Leal, Laminar Flow and Convective Transport Processes, Butterworth Heinemann, Boston, 1992.

[23] D.A. Edwards, Estimating rate constants in a convection-diffusion system with a boundary reaction, IMA J. Appl. Math. 63 (1999) 89.

[24] D.A. Edwards, S.A. Jackson, Testing the validity of the effective rate constant approximation for surface reaction with transport, Appl. Math. Lett. 15 (2002) 547.

[25] D.A. Edwards, Surface reaction near a stagnation point, Stud. Appl. Math. 105 (2000) 1.

[26] D.A. Edwards, Biochemical reactions on helical structures, SIAM J. Appl. Math. 60 (2000) 1425.

[27] R. Baggio, G.J. Carven, A. Chiulli, M. Palmer, L.J. Stern, J.E. Arenas, Induced fit of an epitope peptide to a monoclonal antibody probed with a novel parallel surface plasmon resonance assay, J. Biol. Chem. 280 (6) (2005) 4188.

[28] K. Usui-Aoki, K. Shimada, M. Nagano, M. Kawai, H. Koga, A novel approach to protein expression profiling using antibody microarrays combined with surface plasmon resonance technology, Proteomics 5 (9) (2005) 2396.

[29] D.A. Edwards, The effect of a receptor layer on the measurement of rate constants, Bull. Math. Bio. 63 (2001) 301.

[30] L. Lewin, Polylogarithms and Associated Functions, North Holland, Amsterdam, 1981.

[31] M. Abramowitz, I.A. Stegun (Eds.), Handbook of Mathematical Functions, Applied Mathematics Series, vol. 155, U.S. Dept. of Commerce, Washington, 1972.

[32] R.B. Bird, W.E. Stewart, E.N. Lightfoot, Transport Phenomena, Wiley, New York, 1960.